*Journal of Advanced Ceramics*
2017, **6**(2): 165–175
DOI: 10.1007/s40145-017-0229-1

ISSN 2226-4108
CN 10-1154/TQ

**Research Article**

# Pressureless sintering of ZrC with variable stoichiometry

Katrin SCHÖNFELD*, Hans-Peter MARTIN, Alexander MICHAELIS

*Fraunhofer Institute for Ceramic Technologies and Systems IKTS, Dresden, Germany*

Received: January 05, 2017; Revised: March 28, 2017; Accepted: April 18, 2017


**Abstract:** This paper presents the experiments on the synthesis of zirconium carbide (ZrC) using carbothermal reduction of zirconia ($ZrO_2$). The ratio of $ZrO_2$:C is used to adapt $ZrC_xO_y$ with $x<1$ or ZrC + C. The modification of $ZrC_xO_y$ and the total carbon amount allows the use of pressureless sintering method in combination with sintering temperatures ⩽ 2000 ℃. Fully densified ZrC products are obtained. The relevant details of ZrC formation are investigated by X-ray diffraction (XRD). The sintered products are characterized by XRD, field emission scanning electron microscopy (FESEM), as well as mechanical and electrical methods. XRD and FESEM investigations show that $ZrC_xO_y$ is formed during the manufacturing process. The grain size and additional zirconia or carbon are related to the $ZrO_2$:C ratio of the starting powder mixture. Bending strength up to 300 MPa, Young's modulus up to 400 GPa, fracture toughness up to 4.1 MPa·$m^{1/2}$, and electrical resistance at room temperature around $10^{-4}$ Ω·cm are reached by the pressureless sintered ZrC.

**Keywords:** zirconium carbide (ZrC); carbothermal reduction; sintering; mechanical properties; electrical properties

## 1 Introduction

In theory, zirconium carbide shows similar advantageous high-temperature/high-vacuum resistance and a superior chemical resistance as tungsten and molybdenum metals. Therefore, it is attractive to substitute those strategic metals with zirconium carbide. In order to use the products of ZrC, it is necessary to develop an economic manufacturing technology. The poor sinterability, due to solid phase sintering of ZrC, is a challenge for the establishment of bulk ZrC products on the market. In the past, a combination of very high-temperature with pressure-assisted methods was necessary to produce fully densified ZrC components. Hot pressing is a common method for sintering of ZrC [1–6]. Nachiappan *et al*. [4] investigated the influence of Zr and graphite ratio on sinterability. A high Zr:C ratio promotes the sinterability as it is shown by this paper. Wang *et al*. [5] added Zr or C for ZrC hot pressing experiments at temperatures between 1800 and 2000 ℃. The relative density of pure ZrC materials sintered at 2000 ℃ reaches 83%. Adding elemental Zr to ZrC increases the densification level. It is supposed that the formation of $ZrC_{0.9}$ by incorporation of Zr in ZrC promotes the sintering process. Nevertheless, an undesirably exaggerated grain growth occurs with the addition of Zr. Other authors demonstrate an improvement of ZrC sinterability by addition of $ZrB_2$ and SiC [7–10]. An alternative sintering method, which enables high densification of ZrC material, is spark plasma sintering (SPS). However, it is not as productive as pressureless sintering. There are other papers, which consider the sintering mechanism of bulk ZrC using oxycarbide $ZrC_xO_y$ powders. The enhanced Zr lattice diffusion promotes the sintering behavior and improves

* Corresponding author.
E-mail: katrin.schoenfeld@ikts.fraunhofer.de

the densification process for these powders [11–13].

Few investigations were performed concerning pressureless sintering of ZrC until now. Silvestroni and Sciti [14] densified ZrC-based materials by pressureless sintering applying up to 20 vol% $MoSi_2$ addition. That paper reports a maximum of 97% theoretical density after sintering at 1900–1950 ℃. Zhao *et al*. [15] reached a densification of 98.4% at 2100 ℃ for ZrC powders without any additives but extensive high-energy milling. Additives of graphite and SiC enable the decrease of the sintering temperature and limit the grain growth additionally. The previous research by other authors reached improvement of ZrC sinterability by

(1) application of chemically different additives, which deteriorates the high-temperature properties of ZrC;

(2) high-energy milling, which requires additional technological effort;

(3) use of oxycarbide ($ZrC_xO_y$), which restricts the high-temperature stability of the sintered products.

This paper reports the development of an improved pressureless sintering process for ZrC ceramics. Technological and economic advantages are achieved with regard to the previously described manufacturing routes. The combination of high-energy ball milling, the use of economic starting powders, plus the temporary formation of modified ZrC powders with carbon deficiency, are the key to full densification of ZrC without applying pressure.

Basic investigations were conducted with regard to sub-stoichiometry or incorporation of oxygen for ZrC (meaning $ZrC_xO_y$ with $x<1$, $y \ll 1$) powder processing and promotion of ZrC sintering by additives [4,5,9,15–17]. These papers discuss specific effects of $ZrC_xO_y$ composition in relation to sintering behavior. The reaction of $ZrO_2$ and C tends to produce $ZrC_xO_y$ with $0<x<1$, $y>0$ and $x+y \leqslant 1$ as long as the reaction is incomplete due to kinetic reasons. Oxygen atoms could easily occupy the carbon positions in the Zr–C lattice [13,18,19]. However, the thermodynamically stable situation will be a sub-stoichiometric $ZrC_xO_y$ with $x<1$, $y=0$, which is hard to achieve. Therefore, the final $ZrC_xO_y$ will become $ZrC_xO_y$ with $x<1$, $y \approx 0$. Our own experiments indicate that sub-stoichiometric $ZrC_xO_y$ could substantially promote the sintering progress of zirconium carbide, which is in accordance with Ref. [13]. Our approach tries to combine powder processing and sub-stoichiometry effects to establish a more economic manufacturing route for dense zirconium carbide ceramics. Most important goals, which are associated with economic and technical issues, are

(1) sintering temperature (preferably ⩽ 2000 ℃);

(2) density after sintering (preferably > 95 % in theory).

A much more reactive ZrC as described in Ref. [20] can be obtained from the reduction of commercially available very fine-grained $ZrO_2$ at about 1600 ℃ [21]. To produce $ZrC_xO_y$ with high sinterability, a defined limitation of the C content in the powder mixture is recommended (1a):

$$ZrO_2 + 3C \rightarrow ZrC + 2CO \quad (1)$$

$$ZrO_2 + (2+x-y)C \rightarrow ZrC_xO_y + (2-y)CO,\ x<1 \quad (1a)$$

$$ZrC_xO_y \rightarrow ZrC_{x-y} + yCO \quad (1b)$$

Theoretically, the final product is zirconium-rich zirconium carbide as indicated by reaction (1b). Residual oxygen probably keeps its position in the Zr–C lattice even at very high temperatures. $ZrC_xO_y$ is significantly more active in sintering than the stoichiometric ZrC. However, the best option in sintering for the $x$ level is unknown for technological reasons and needs to be explored experimentally.

A further step towards excellent sintering behavior is the exclusion of any gas-producing reaction as can be seen for reactions (1), (1a), and (1b).

The present publication shows that it is possible to sinter ZrC components densely with relatively little effort. With the aid of the outlined technology, components with relatively good mechanical and electrical properties were produced. In order to establish this technology as an industrial process, further improvements and optimization regarding powder preparation, composition, and temperature profile of synthesis and sintering are necessary. The determination of mechanical and electrical properties needs to be deepened, and investigations regarding chemical corrosion and wear resistance have to be conducted. Those challenging requirements will be addressed in future work.

## 2 Materials and methods

### 2. 1 Preparation of ceramic powders

$ZrO_2$ (Treibacher, $d_{50}=800$ nm) and carbon black powders (Overlack, $d_{50}=60$ nm) were used as starting materials for our experiments. The ratio of zirconia and

**Table 1 Composition of investigated $ZrO_2$–C mixtures**

| Sample | $ZrO_2$ (wt%) | C (wt%) | $ZrO_2$:C molar ratio |
|---|---|---|---|
| ZC 1-3.2 | 75.8 | 24.2 | 1:3.20 |
| ZC 1-3.1 | 76.8 | 23.2 | 1:3.10 |
| ZC 1-3.0 | 77.3 | 22.7 | 1:3.00 |
| ZC 1-2.9 | 77.9 | 22.1 | 1:2.89 |
| ZC 1-2.8 | 78.7 | 21.3 | 1:2.78 |
| ZC 1-2.7 | 79.2 | 20.8 | 1:2.70 |
| ZC 1-2.6 | 79.8 | 20.2 | 1:2.60 |

carbon was varied as shown in Table 1. These starting ratios were used for all the samples in this publication. The aqueous suspension was freeze dried and granulated after 6 h ball milling. The obtained powder mixture of $ZrO_2$ and C was transformed into $ZrC_xO_y$ at 1700 ℃ under argon atmosphere. The dwell time at 1700 ℃ was 4 h. After transformation, the particle size of the $ZrC_xO_y$ powders was $d_{50} = 2.7$ μm with a specific surface of 2.5 $m^2/g$.

The temperature-dependent conversion state of $ZrO_2$/C mixture into ZrC was analyzed by X-ray diffraction (XRD; Bruker D8, Cu Kα irradiation) after the synthesis process. The XRD patterns in Fig. 1 show the progress of ZrC conversion for $ZrO_2$:C = 1:3.00 with rising temperature. The ZrC transformation is completed at 1600 ℃. A synthesis temperature of 1700 ℃ guarantees a full conversion, even for large powder quantities. The calculation of the ZrC lattice parameter and the phase analysis were performed using XRD analysis software TOPAS version 4.2 by Rietveld method. The milling procedure needs to be repeated after powder synthesis because of a weak particle sintering. Organic waxes were added to the synthesized powders to serve as pressing aid later in the shaping process. The particle size was reduced to $d_{50} = 1.0$ μm with BET = 6.2 $m^2/g$. The synthesized powders and the pressing aid were mixed and ball milled in isopropanol

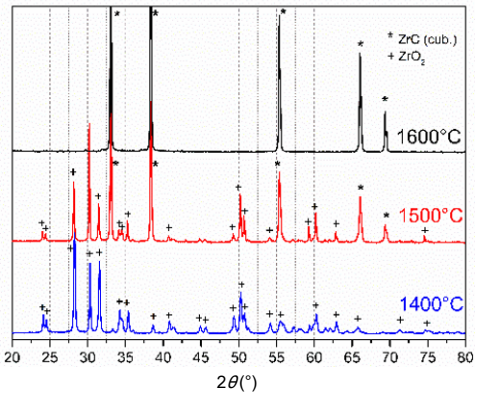


**Fig. 1** XRD patterns of $ZrO_2$ and carbon black powder mixture in the molar ratio of 1:3.00 after synthesis process with synthesis temperature.

for 4 h. After drying of the obtained suspension, a two-step shaping procedure was applied consisting of a primary uniaxial pressing (30 MPa) step and a second cold isostatic pressing (300 MPa) step. The pressing aid was removed by pyrolysis under nitrogen atmosphere at 600 ℃.

## 2.2 Sintering

The pressureless sintering procedure of the specimen was performed in a temperature range of 1850–2000 ℃ under argon atmosphere using an electrically heated graphite furnace. Figure 2 illustrates the complete process flow. The sintered samples were analyzed with regard to

(1) density after sintering;

(2) mechanical properties (strength, hardness, fracture toughness);

(3) electrical resistance;

(4) material morphology (microscopy).

## 2.3 Characterization

The density of the sintered products was analyzed by Archimedes method according to DIN EN 623-2. The mechanical properties were measured by 4-point bending (4PB) test according to DIN EN 843-1 using an UPM testing machine (Hegewald & Peschke). With the machine AVK-C2 type HV5, the hardness was tested according to DIN 843-4. The fracture toughness was calculated from crack length by Shetty algorithm. The Young's modulus was measured in accordance with ASTM E1876-99.

Ceramographic cross sections were prepared and used to analyze grain size, grain shape, and porosity of

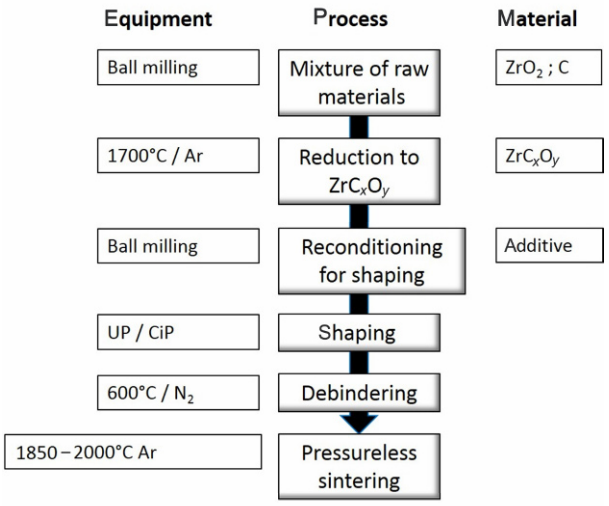


**Fig. 2** Process flow of ZrC preparation.

the sintered ZrC material by field emission scanning electron microscopy (FESEM; Leica S260). Additional analysis of materials was conducted using energy-dispersive X-ray spectroscopy (EDX; ISIS Si (Li) detector). XRD was analyzed with Bruker D8 diffractometer with position sensitive detector (PSD) and Cu Kα radiation ($\lambda = 1.54056$ Å).

Electrical resistivity was measured as stated in DIN 51911 using inert gas atmosphere for the measurement up to 2000 ℃. 4-probe method was applied for electrical resistivity measurements up to 1000 ℃ under inert gas as well as a heating rate of 5 K/min. Keithley 2611A supplied a well-defined currency and the resulting voltage was measured by Keithley 2182A.

The carbon content was determined according to DIN EN ISO 9556 with LECO CS230 analyzer, and the oxygen content with LECO TCH600 according to DIN ISO 4491.

## 3 Results and discussion

### 3. 1 Chemical composition

The reduction of $ZrO_2$ by C was used to produce $ZrC_xO_y$. The crystallographic parameters of $ZrC_xO_y$ oxycarbide [13] and reduced $ZrC_x$ powders with non-stoichiometric composition [22] were reported in literature before. A shift of the lattice parameter is observed for both alternatives of ZrC in the same direction. Our experiments (Fig. 3) reproduce that shift in correlation with the alteration of the starting composition with $ZrO_2$:C in the range of 1:2.60 to 1:3.20 (samples ZC 1-2.6,…, ZC 1-3.2). The (220) and (200) peaks of cubic ZrC were used to illustrate the peak shift (Fig. 3). The $ZrC_xO_y$ peak position shifts to a higher diffraction angle. Sample ZC 1-2.7 derived from the starting $ZrO_2$:C composition of 1:2.70 changes to $2\theta = 55.57°$ ($d = 1.65241$ Å). The peak of the carbon-rich starting powders ZC 1-3.1 ($ZrO_2$:C = 1:3.10) shifts to a lower angle of $2\theta = 55.27°$ ($d = 1.6066$ Å). According to the phase diagram of Zr–C (Fig. 4), the peak shift appears for the composition $ZrO_2$:C = 1:3.00–1:2.70 because no further change of the Zr–C lattice can be expected.

The observed peak shift either indicates the Zr:C ratio or the Zr:C:O composition of the synthesized powders.

The ZrC lattice parameter and phase analysis were determined by Rietveld method with XRD analysis software TOPAS version 4.2. The program calculation

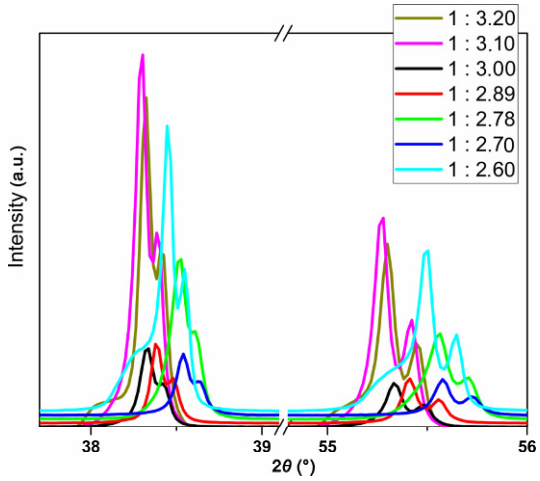


**Fig. 3** *hkl* peak = 200 (diffraction between 38° and 39°) and *hkl* peak = 220 (diffraction between 55° and 56°) with peak shift of different powder compositions (Cu Kα, $\lambda$ = 1.54056 Å).

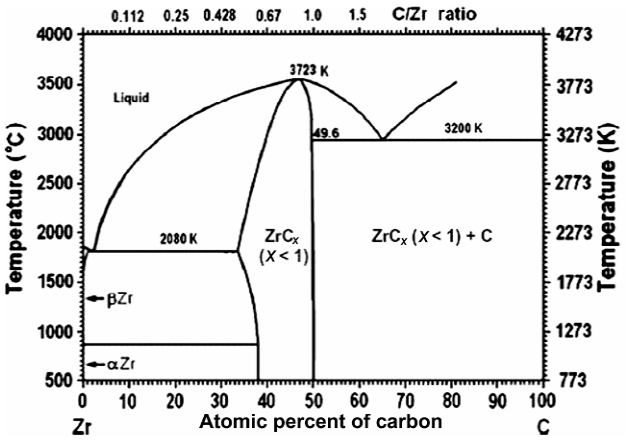


**Fig. 4** Phase diagram of Zr–C system (reproduced with permission from Ref. [23], © 2013 Elsevier B.V.).

for the lattice constant $a$ of the associated ZrC lattice-based $d$ was derived from all peaks and Bragg equation in combination with (*hkl*) numbers associated with $d$.

$$d = \frac{n}{2} \cdot \frac{\lambda}{\sin\theta}$$

$$a = \sqrt{h^2 + k^2 + l^2} \cdot d$$

The lattice distance in relation to the $ZrO_2$:C ratio is illustrated in Fig. 5.

The lattice parameter of stoichiometric ZrC, meaning the Zr:C molar ratio is 1:1, is 4.69764 Å [24]. According to the phase diagram, ZrC exists within the composition range of 38–50 at% C. The maximum carbon content within the ZrC lattice is the stoichiometric ZrC. The minimum carbon content is the composition $ZrC_{0.76}$. A shift of the lattice parameter of 4.69764 to 4.6823 Å can be related either to a lack of

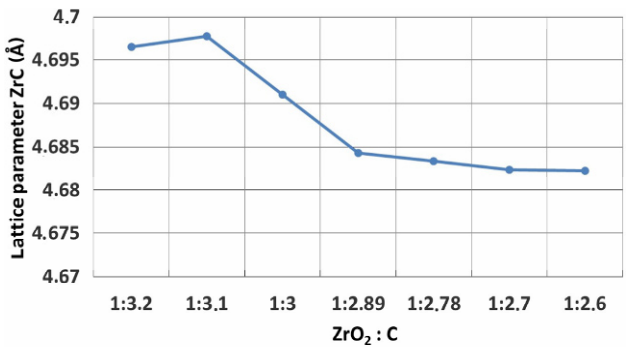


**Fig. 5** Lattice distance of ZrC in relation to $ZrO_2$:C ratio.

carbon or to a substitution of carbon in the lattice by oxygen. Both will lead to a decrease of the lattice constant.

Observations show that the lattice constant of stoichiometric ZrC is only reached by the starting compositions $ZrO_2$:C > 3. As an explanation, more carbon is required because of a kinetically caused, incomplete carbon reaction with $ZrO_2$. Therefore, it is necessary to add more carbon as theoretically required to obtain the stoichiometric ZrC composition. The constant lattice parameter for $ZrO_2$:C = 1:3.10 and 1:3.20 proves that no additional carbon can be incorporated into the ZrC lattice. Less carbon leads to a lack of carbon in the ZrC lattice and a decrease of the lattice parameter towards a minimum of 4.685 Å indicating the formation of $ZrC_xO_y$ compound with $x$ < 1. The incomplete reaction could lead to different compositions of the final product:

(1) $ZrC_xO_y$ with $x < 1 + ZrO_2$;

(2) $ZrC_xO_y$;

(3) $ZrC_x + ZrO_2$.

Consequently, a chemical analysis of oxygen in combination with an XRD phase analysis was performed. The results of the oxygen and carbon analysis are shown in Table 2. The chemical analysis detects considerable amount of oxygen. However, this analysis does not distinguish between the oxygen in $ZrC_xO_y$ and $ZrO_2$. On the other hand, the XRD data can only supply a rough orientation about phase content. Therefore, C, $ZrO_2$, and $ZrC_xO_y$ phase composition and content can only be roughly estimated by the available data from our investigations.

**Table 2 Chemical analysis results**

| $ZrO_2$:C | Zr (wt%) | Zr (mol%) | C (wt%) | C (mol%) | O (wt%) | O (mol%) |
|---|---|---|---|---|---|---|
| 1:3.00 | 87.47 | 48.33 | 11.63 | 48.84 | 0.90 | 2.82 |
| 1:2.78 | 88.16 | 50.81 | 9.43 | 41.25 | 2.41 | 7.93 |

$ZrO_2$ phase can be distinguished from the other phases by XRD but the obtained data from the Rietveld analysis are linked with a significant imprecision, which needs to be considered. The $ZrO_2$ amount, which is calculated from XRD data (Table 3), produces the information about the oxygen and zirconium bound in the oxide. The residual $ZrO_2$ content of samples ZC 1-3.0, ZC 1-3.1, and ZC 1-3.2 is nearly zero, which was to be expected after sample set up. The difference in the numerical value occurs due to measurement imprecision. The residual oxygen and zirconium can be expected in a $ZrC_xO_y$ phase. The completely characterized samples ZC 1-3.0 and ZC 1-2.8 can be assessed by the use of the data in Tables 2 and 3. The calculated results are

(1) ZC 1-3.0 0.15 wt% $ZrO_2$ 99.85 wt% $ZrC_{1.01}O_{0.05}$;

(2) ZC 1-2.8 1.61 wt% $ZrO_2$ 98.39 wt% $ZrC_{0.83}O_{0.14}$.

Therefore, it can be assumed that the zirconium carbide consists of a variable $ZrC_xO_y$ phase and residual zirconium oxide. Subsequently, it is probable that the decrease of the lattice parameter is mainly associated with $ZrC_xO_y$ formation (option (1)).

The XRDs of the synthesized powders clearly show that residual zirconia can be detected in the samples derived from the $ZrO_2$:C mixtures with less carbon than 2.78 (Fig. 6). This result corresponds with a final composition of $ZrC_xO_y$ + $ZrO_2$. The complete oxygen from $ZrO_2$ of the starting mixture is removed by reduction for mixtures with carbon content of 2.9, and only $ZrC_xO_y$ with $x < 1$ is formed. $ZrC_xO_y$ with $x \approx 1$, $y \approx 0$ is formed from mixtures with carbon content of more than 3.00.

## 3. 2 Structural analysis

The SEM cross section images of sintered ZrC materials at 1900 and 2000 ℃ are illustrated in Fig. 7. Figures 7(a) and 7(b), which are attributed to the sintered sample derived from starting powders of $ZrO_2$:C = 1:3.00, do not indicate any extrinsic phase like $ZrO_2$ or C. This is compatible with the results from the

**Table 3 $ZrO_2$ content after reduction according to XRD phase analysis**

| Sample | $ZrO_2$:C | $ZrO_2$ content (wt%) | Amount of oxygen in $ZrO_2$ (wt%) |
|---|---|---|---|
| ZC 1-3.2 | 1:3.20 | 0.19 | 0.05 |
| ZC 1-3.1 | 1:3.10 | 0.22 | 0.06 |
| ZC 1-3.0 | 1:3.00 | 0.15 | 0.04 |
| ZC 1-2.9 | 1:2.89 | 1.10 | 0.29 |
| ZC 1-2.8 | 1:2.78 | 1.61 | 0.42 |
| ZC 1-2.7 | 1:2.70 | 4.37 | 1.14 |
| ZC 1-2.6 | 1:2.60 | 5.10 | 1.32 |

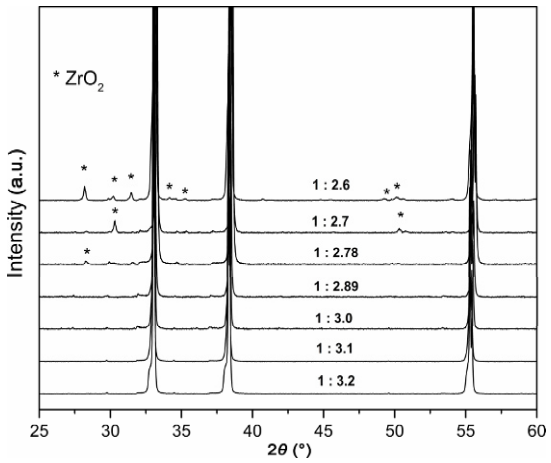


**Fig. 6** XRD patterns of different powder composition.

XRD analysis and chemical analysis. It fits exactly the expectations from literature. Moreover, the residual porosity is considerable for both sintering temperatures (1900 ℃ and 2000 ℃). The amount of pores decreases with increasing sintering temperature, as it is conformable with density results. Additionally, the grain size seems little affected by the increase of the sintering temperature from 1900 to 2000 ℃, which hints to low sinterability of the powders ZC 1-3.0.

Figures 7(c) and 7(d) are attributed to the sintered sample derived from the starting powders with composition $ZrO_2$:C = 1:2.60. $ZrO_2$ residuals can be detected at the grain boundaries and triple points of the grains for both sintering temperatures. This confirms the similar probability of both interpretation options for

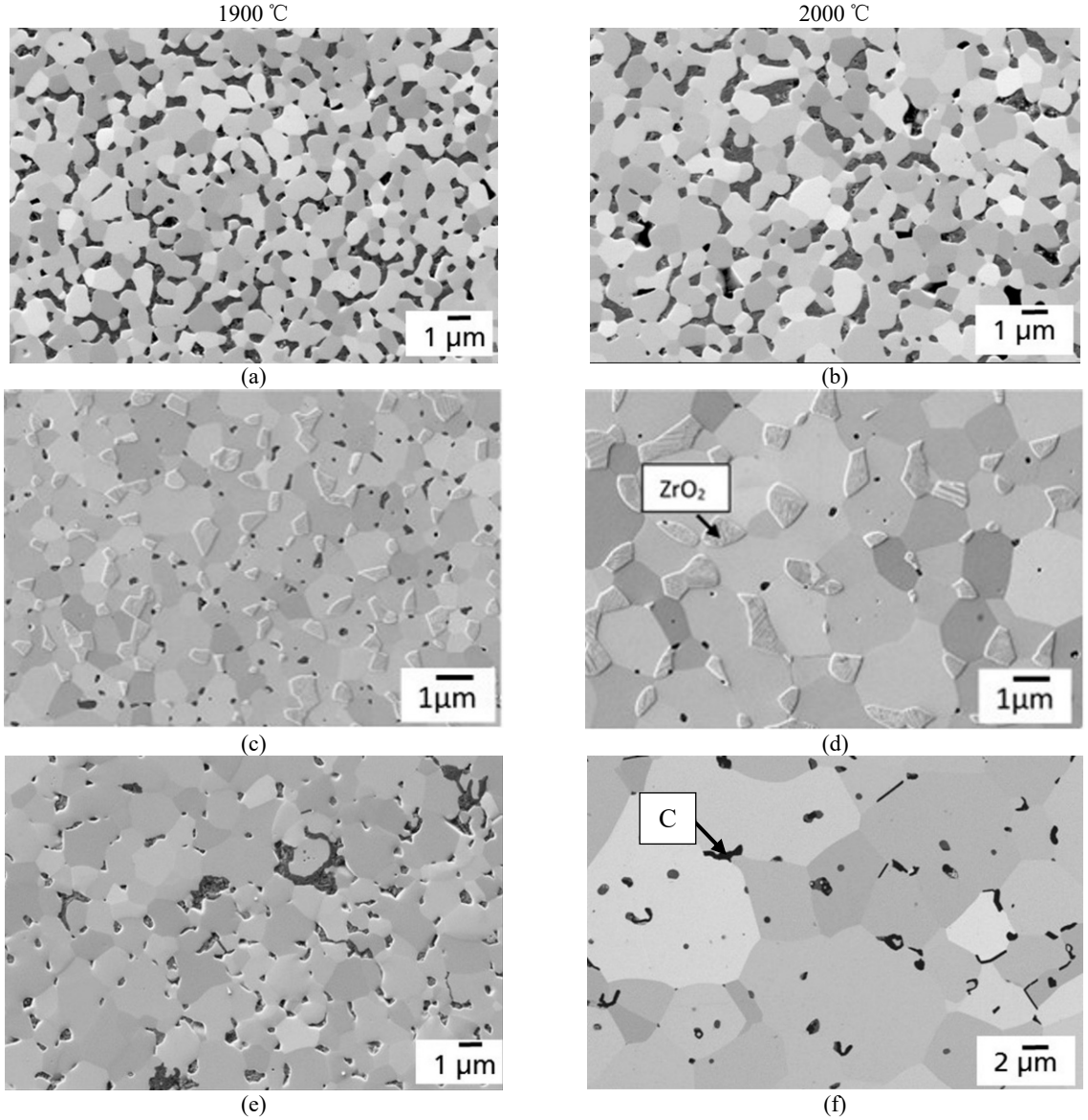


**Fig. 7** (a) ZC 1-3.0, ZrC 1900 ℃; (b) ZC 1-3.0, ZrC 2000 ℃; (c) ZC 1-2.6, ZrC 1900 ℃; (d) ZC 1-2.6, 2000 ℃; (e) ZC 1-3.2, ZrC 1900 ℃; (f) ZC 1-3.2, ZrC 2000 ℃.

the XRD data as either a peak shift caused by lack of C in $ZrC_xO_y$ or oxygen integration in the ZrC lattice.

A reduction of $ZrO_2$ may be caused by thermodynamic stabilization of $ZrC_xO_y$–$ZrO_2$ composition or by kinetical output of the reaction. The observed $ZrO_2$ particles are more or less included within the ZrC grains, which may have stopped the conversion process. The kinetical output for $ZrO_2$ residues could be experimentally proven by investigations with prolonged sintering time. Another observation is the increase of grain size in association with increased sintering temperature for this sample. 1900 ℃ sintering temperature produces grains with sizes a little larger than that of the sample of $ZrO_2$:C = 1:3.00 and instead of pores $ZrO_2$ particles are in the grain boundaries. That is why the density for this sample (94.6% theoretical density) is much higher than the 86% theoretical density of the 1:3.00 composition. Growth of the grain size up to 5 μm and decrease of the amount of pores by sintering at 2000 ℃ are observed. The sinterability of the powders of $ZrO_2$:C = 1:2.60 is definitely increased in comparison with the 1:3.00 one.

Figures 7(e) and 7(f) are attributed to starting materials of $ZrO_2$:C = 1:3.20. Carbon residuals occur at the grain boundaries instead of the oxides before. A significant grain growth obviously occurs at 1900 ℃ already and continues at 2000 ℃. The absence of $ZrO_2$ is certainly related to the excess of carbon in the samples.

### 3. 3 Mechanical properties

A complete data set concerning density, grain size, and mechanical properties of the manufactured ZrC samples is presented in Table 4. In Fig. 8 and Fig. 9, the correlation between sintering temperature and density as well as Young's modulus and 4PB strength are illustrated. For better review, one sample of the $ZrO_2$:C ratio less than 1:3.00 and one sample of the $ZrO_2$:C ratio higher than 1:3.00 were chosen.

The material density after sintering is a simple indicator of the state of sintering. The density data of Table 4 clearly demonstrate the effect of the $ZrO_2$:C ratio and the sintering temperature. Additionally, the graphs of Fig. 8 illustrate those effects. The ZC 1-3.0 sample has a significant lower density than the other samples, which confirms the low sinteractivity of the composition $ZrO_2$:C = 1:3.00 again. The maximum density of this composition reaches 86% of theoretical density (6.73 g/cm$^3$) after 2000 ℃ sintering temperature. A remarkable increase of density is observed when changing the $ZrO_2$:C composition ratio of the starting powder mixture. Higher sintering activity can be obtained either by decreasing or increasing the carbon content of the starting material. The physical reason for this observation is that the lattice sites of ZrC are not completely occupied by carbon atoms in the case of low carbon content. The lattice vacancies enable higher diffusion velocity of atoms which promotes the sintering process. In the case of excess carbon, the carbon components enable higher diffusion velocity which enables higher sintering activity in a similar way.

The normal effect of increased sintering temperatures is the promotion of densification and grain growth. Almost completely densified ZrC can be obtained at 2000 ℃ by either a carbon excess or a carbon lack approach.

**Table 4 Mechanical properties, grain size, and density for all prepared samples**

| $ZrO_2$:C | Sintering temperature (℃) | Theoretical density (%) | $K_{Ic}$ (Shetty) (MPa·m$^{1/2}$) | HV5 (GPa) | 4PB (MPa) | Young's modulus (GPa) | Grain size (μm) |
|---|---|---|---|---|---|---|---|
| 1:3.20 | 1850 | 79.97 | 2.4 | 6.39 | 190.6 | 199.56 | 0.1–0.8 |
| | 1900 | 91.97 | 3.6 | 11.99 | 284.3 | 317.12 | 0.6–2.3 |
| | 2000 | 97.75 | 4.0 | 14.81 | 308.6 | 374.27 | 1.0–7.0 |
| 1:3.10 | 1850 | 82.46 | 3.5 | 12.13 | 271.6 | 285.79 | 0.3–0.9 |
| | 1900 | 89.44 | 4.0 | 15.17 | 294.6 | 364.69 | 0.3–1.2 |
| | 2000 | 98.56 | — | — | 287.0 | 406.71 | 3.9–30.9 |
| 1:3.00 | 1900 | 78.00 | — | — | 196.0 | 200.30 | 0.5–2.0 |
| | 2000 | 86.00 | — | — | 214.0 | 249.70 | 0.5–2.2 |
| 1:2.89 | 1900 | 85.60 | — | — | 165.0 | | 0.7–3.0 |
| | 2000 | 95.80 | — | — | 251.0 | | 0.5–2.4 |
| 1:2.78 | 1900 | 92.30 | 3.3 | 13.06 | 201.0 | | 0.7–2.3 |
| | 2000 | 100.90 | 3.6 | 14.87 | 235.0 | | 2.1–4.8 |
| 1:2.70 | 1850 | 87.45 | 2.7 | 9.09 | 195.3 | | 0.4–1.2 |
| | 1900 | 92.60 | 3.2 | 11.53 | 239.0 | 306.00 | 0.6–2.3 |
| | 2000 | 97.90 | 4.0 | 14.53 | 259.33 | 361.30 | 0.9–4.5 |
| 1:2.60 | 1850 | 89.50 | 2.8 | 10.03 | 192.7 | | 0.3–1.0 |
| | 1900 | 94.60 | 3.7 | 13.31 | 246.0 | | 0.4–3.2 |
| | 2000 | 98.90 | 4.1 | 14.43 | 309.0 | | 1.5–4.9 |

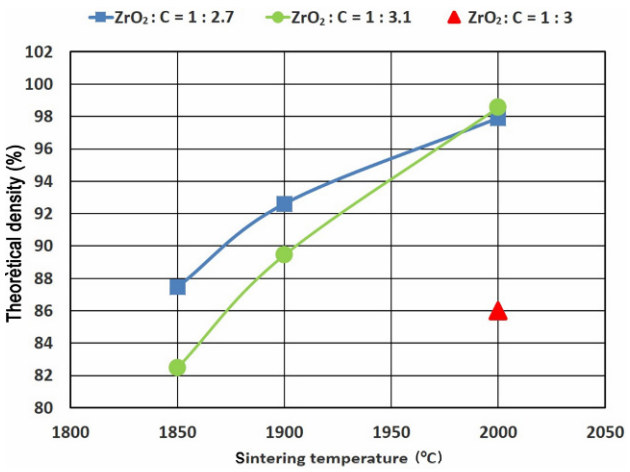


**Fig. 8** Densification of ZrC material with different stoichiometry.

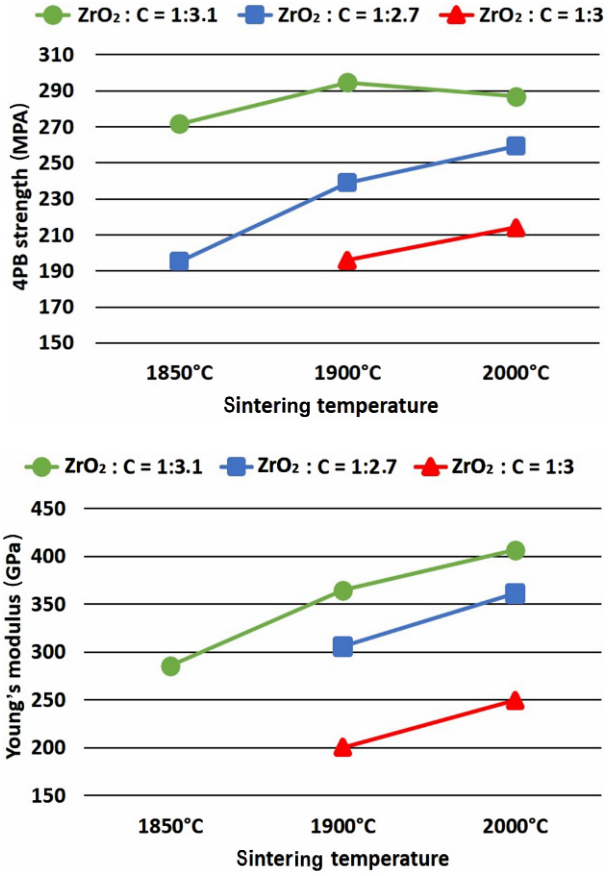


**Fig. 9** Young's modulus (bottom) and 4PB strength (up) of pressureless sintered ZrC material according to sintering temperature.

A second indicator of sintering activity is the final grain size of the material. The starting grain size of the synthesized powders is roughly in the range of 0.5–1.0 μm. A sintering temperature < 2000 ℃ does not cause a significant grain growth for most samples. Nevertheless, remarkable high density can be reached by use of low carbon-containing mixtures (ZC 1-2.6). A sintering temperature of 2000 ℃ always leads to a remarkable increase of the ZrC grains except for the stoichiometric composition of sample ZC 1-3.0. A low carbon amount promotes grain growth up to around 5 μm maximum size. A high carbon content can promote the grain growth even more, up to a size significantly above 10 μm. This corresponds exactly to the results of density data.

The density and the grain size structure strongly affect the mechanical and electrical properties. The data of Young's modulus, 4-point bending strength, and fracture toughness are shown in Fig. 9 and Fig. 10, respectively. Cheng *et al*. [25] calculated the theoretical Young's modulus of ZrC with 473 GPa. Landwehr *et al*. [3] achieved 400 GPa by hot pressing of dense ZrC–Mo cermet. A review paper [26] reports ZrC data for Young's modulus between 380 and 407 GPa. The results of this paper range from 200 to 406 GPa. Samples manufactured at low sintering temperatures reach a lower Young's modulus than those produced at higher sintering temperatures. The low level of the samples sintered below 2000 ℃ is certainly derived from the high amount of porosity. The effect of the $ZrO_2$:C ratio of the starting mixture and finally the oxygen amount of $ZrC_xO_y$ is not verifiable. The ruling influence on the Young's modulus is the porosity/density of the samples. Fully dense samples reach a level of around 400 GPa as it is reported in the literature for hot-pressed samples of ZrC.

The bending strength is increased by decreasing the porosity and grain size. Due to sintering, a decrease of porosity and grain growth is happening. Regarding the bending strength, these two processes are oppositionally affected. In our case, an increase of bending strength was detectable, meaning the porosity seems to have a higher influence than the grain size. The balance of both is required to obtain a high level of strength. Maximum strength is reached by samples of ZC 1-3.2 composition. The additional carbon component improves the strength of the material compared to the samples with $ZrO_2$:C < 1:3.00. Here the additional $ZrO_2$ phase in the tribble junction of ZrC structure is lowering the 4PB strength. Sample ZC 1-3.1 demonstrates that a huge grain size can overcompensate the effect of decreased porosity in strength. However, moderate strength was reached for all samples by sintering at temperature of 2000 ℃. A

level of 200 MPa as result of 4-point bending test is an acceptable quality for technical applications.

The fracture toughness was calculated from crack length of HV5 imprint by Shetty algorithm. The hardness itself also depends on the density of the material as shown in Table 4. Fracture toughness often limits the application fields of ceramic materials. An average ceramic level is reached with $K_{Ic} > 3$ MPa·m$^{1/2}$. A sintering temperature of 1900 ℃ produces ZrC samples with $K_{Ic} \approx 3.5$ MPa·m$^{1/2}$. The influence of the grain size and crack formation needs more investigations than shown in Fig. 10. The current impression is that medium-sized grains of about 5 μm can increase the fracture toughness from 3 to 4 MPa·m$^{1/2}$. This is an acceptable base for numerous applications. Crack toughness data with $K_{Ic} = 3.3$ MPa·m$^{1/2}$ for SPS sintered ZrC were found in literature from previous work of Sagdic *et al*. [27]

Two types of electrical resistance investigations were performed. The first measurement used a setup which allows test temperatures up to 2000 ℃ on large samples (150 mm in length). The obtained curve of this test confirms a linear increase of electrical resistance up to the maximum temperature. Additionally, it proves the stability of the sintered ZrC. The second test is the 4 probe test up to 1000 ℃. Smaller samples (20 mm in length) are heated up by an external heater. The reference material for the 4 probe measurements is tungsten. The obtained data correspond perfectly with literature data of tungsten and the 2000 ℃ test. Figure 11 illustrates that ZrC resistance is about one magnitude above the tungsten resistance. A slight difference can be seen between ZrC derived from $ZrO_2$ and C mixtures with high or low carbon amount and the 1:3.00 mixture which is supposed to produce stoichiometric ZrC. The difference between the $ZrC_xO_y$ samples may be explained rather by the porosity than composition alteration of $ZrC_xO_y$. The temperature behavior reminds of metallic behavior as it is expected for ZrC material. The increase of electrical resistance is about twice between room temperature and 2000 ℃.

## 4 Conclusions

The first step of ZrC ceramic manufacturing is the carbothermal reduction of $ZrO_2$ as described in this paper. The starting powders can be adjusted with

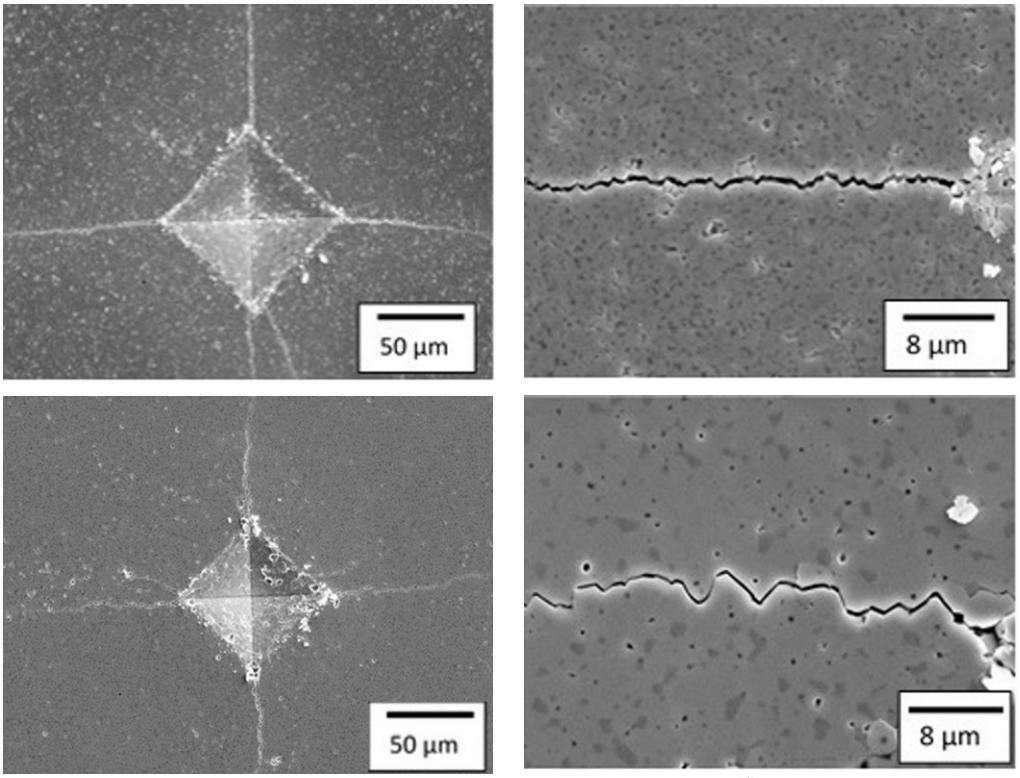


**Fig. 10** Vickers imprint and crack path in ZrC samples: calculated $K_{Ic} = 2.8$ MPa·m$^{1/2}$ for ZC1-2.6 sintered at 1850 ℃ with maximum grain size of 1 μm (upper pictures), and calculated $K_{Ic} = 4.1$ MPa·m$^{1/2}$ for ZC1-2.6 sintered at 2000 ℃ with maximum grain size of 5 μm (lower pictures).

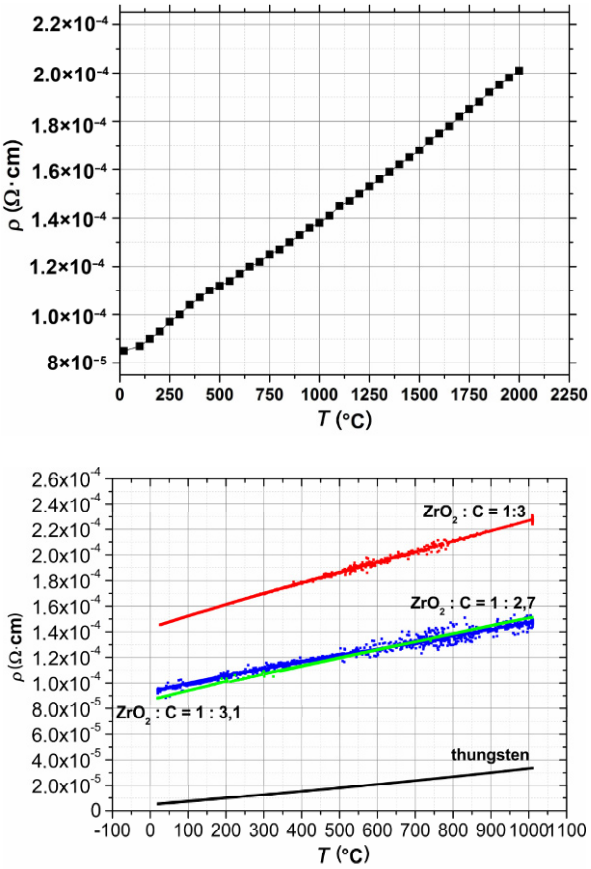


**Fig. 11** Electrical resistivity of ZC 1-2.8 sintered at 2000 ℃ in dependence of temperature up to 1000 ℃ (bottom) and 2000 ℃ (up).

different $ZrO_2$:C ratios to produce different $ZrC_xO_y$ powders with $x \leqslant 1$ and $y \approx 0, \ldots, y < 0.2$.

The paper demonstrates that $ZrC_xO_y$ can be sintered by pressureless sintering. The most efficient lever to increase the sintering activity of ZrC is the modification of the starting powders. Dramatic change in sintering behavior is obtained by changing the $ZrO_2$:C ratio. It is possible to get fully densified ZrC materials without any sintering additives already at a temperature of 2000 ℃. The experiments show that the increase of the sintering temperature together with the $ZrO_2$:C ratio efficiently promotes the sintering.

The grain size of the produced ZrC materials depends on sintering temperature and $ZrO_2$:C ratio of the starting powders. In the case of $ZrO_2$:C = 1:3.00, no significant grain growth was observed for the applied sintering temperatures. Other $ZrO_2$:C ratios lead to considerable grain growth with increasing sintering temperature. Depending on the starting composition $ZrO_2$:C < 1:3.00 or > 1:3.00, either $ZrO_2$ or carbon residues are found by microscopy and XRD.

The manufactured samples were analyzed regarding their mechanical and electrical properties. The obtained mechanical properties of ZrC are close to common advanced ceramics like silicon carbide materials. 4-point bending strength ranges between 200 and 300 MPa. The Young's modulus reaches a level between 300 and 400 GPa. The fracture toughness achieves values between 3 and 4 MPa·$m^{1/2}$.

The electrical properties were investigated by 4 probe method and an additional heating experiment up to 2000 ℃. The electrical resistance was compared with tungsten as a reference material. ZrC shows an electrical resistance, which is roughly one order of magnitude higher than tungsten. The different $ZrC_xO_y$ materials show very similar electrical resistance if $x \neq 1$. $ZrC_xO_y$ material with $x = 1$ exhibits the highest electrical resistance. This increase of electrical resistance is probably caused by the higher number and volume of pores in the ZC 1-3.0 sample and is not an effect of different $ZrC_xO_y$ composition. At this stage of development, it is not possible to decide if $ZrO_2$:C > 1:3.00 or < 1:3.00 is favorable for application, for instance, as heater. For this decision, more data regarding electrical and thermal properties as well as global mechanical properties, also after exposure on application conditions, are necessary.

The found material data and the newly developed manufacturing technology enable the use of ZrC as substitute for tungsten in heater applications. The high thermal resistance up to 2000 ℃, the extremely low vapor pressure, and the perfect electrical properties are favorable for heating elements under vacuum atmosphere.

## References

[1] Barnier P, Brodhag C, Thevenot F. Hot-pressing kinetics of zirconium carbide. *J Mater Sci* 1986, **21**: 2547–2552.

[2] Chakrabarti T, Rangaraj L, Jayaram V. Effect of zirconium on the densification of reactively hot-pressed zirconium carbide. *J Am Ceram Soc* 2014, **97**: 3092–3102.

[3] Landwehr SE, Hilmas GE, Fahrenholtz WG, *et al*. Microstructure and mechanical characterization of ZrC–Mo cermets produced by hot isostatic pressing. *Mat Sci Eng A* 2008, **497**: 79–86.

[4] Nachiappan C, Rangaraj L, Divakar C, *et al*. Synthesis and densification of monolithic zirconium carbide by reactive hot pressing. *J Am Ceram Soc* 2010, **93**: 1341–1346.

[5] Wang X-G, Guo W-M, Kan Y-M, *et al*. Densification behavior and properties of hot-pressed ZrC ceramics with Zr and graphite additives. *J Eur Ceram Soc* 2011, **31**:

1103–1111.
[6] Wang Y, Chen L, Zhang T, *et al*. Effect of iron additive on the sintering behavior of hot-pressed ZrC–W composites. *Key Eng Mater* 2008, **368–372**: 1764–1766.
[7] Rangaraj L, Divakar C, Jayaram V. Reactive hot pressing of $ZrB_2$–$ZrC_x$ ultra-high temperature ceramic composites with the addition of SiC particulate. *J Eur Ceram Soc* 2010, **30**: 3263–3266.
[8] Medri V, Monteverde F, Balbo A, *et al*. Comparison of $ZrB_2$–ZrC–SiC composites fabricated by spark plasma sintering and hot-pressing. *Adv Eng Mater* 2005, **7**: 159–163.
[9] Zhao L, Jia D, Wang Y, Rao J, *et al*. ZrC–$ZrB_2$ matrix composites with enhanced toughness prepared by reactive hot pressing. *Scripta Mater* 2010, **63**: 887–890.
[10] Zimmermann JW, Hilmas GE, Fahrenholtz WG, *et al*. Fabrication and properties of reactively hot pressed $ZrB_2$–SiC ceramics. *J Eur Ceram Soc* 2007, **27**: 2729–2736.
[11] Antou G, Gendre M, Laborde E, *et al*. High temperature compressive creep of spark plasma sintered zirconium (oxy-)carbide. *Mat Sci Eng A* 2014, **612**: 326–334.
[12] Gendre M, Maître A, Trolliard G. A study of the densification mechanisms during spark plasma sintering of zirconium (oxy-)carbide powders. *Acta Mater* 2010, **58**: 2598–2609.
[13] Gendre M, Maître A, Trolliard G. Synthesis of zirconium oxycarbide ($ZrC_xO_y$) powders. Influence of stoichiometry on densification kinetics during spark plasma sintering and on mechanical properties. *J Eur Ceram Soc* 2011, **31**: 2377–2385.
[14] Silvestroni L, Sciti D. Microstruture and properties of pressureless sintered ZrC-based materials. *J Mater Res* 2008, **23**: 1882–1889.
[15] Zhao L, Jia D, Duan X, *et al*. Pressureless sintering of ZrC-based ceramics by enhancing powder sinterability. *Int J Refract Met H* 2011, **29**: 516–521.
[16] Sciti D, Silvestroni L, Nygren M. Spark plasma sintering of Zr- and Hf-borides with decreasing amounts of $MoSi_2$ as sintering aid. *J Eur Ceram Soc* 2008, **28**: 1287–1296.
[17] Sun S-K, Zhang G-J, Wu W-W, *et al*. Reactive spark plasma sintering of ZrC and HfC ceramics with fine microstructures. *Scripta Mater* 2013, **69**: 139–142.
[18] Maitre A, Lefort P. Solid state reaction of zirconia with carbon. *Solid State Ionics* 1997, **104**: 109–122.
[19] Xie J, Fu Z, Wang Y, *et al*. Synthesis of nanosized zirconium carbide powders by a combinational method of sol–gel and pulse current heating. *J Eur Ceram Soc* 2014, **34**: 13.e1–13.e7.
[20] Núñez-González B, Ortiz AL, Guiberteau F, *et al*. Improvement of the spark-plasma-sintering kinetics of ZrC by high-energy ball-milling. *J Am Ceram Soc* 2012, **95**: 453–456.
[21] Kim J-H, Seo M, Park C, *et al*. Effect of two-step reduction on ZrC size and dispersion. *J Alloys Compd* 2015, **633**: 5–10.
[22] Sara RV. The system zirconium–carbon. *J Am Ceram Soc* 1965, **48**: 243–247.
[23] Katoh Y, Vasudevamurthy G, Nozawa T, *et al*. Properties of zirconium carbide for nuclear fuel applications. *J Nucl Mater* 2013, **441**: 718–742.
[24] Kempter CP, Fries JR. Crystallographic data 189: Zirconium carbide. *Anal Chem* 1960, **32**: 570.
[25] Cheng D, Wang, S, Ye H. First-principles calculations of the elastic properties of ZrC and ZrN. *J Alloys Compd* 2004, **377**: 221–224.
[26] Riedel R. *Handbook of Ceramic Hard Materials*. WILEY-VCH Verlag GmbH, 2000.
[27] Sagdic S, Goller G. Densification behavior and mechanical properties of spark plasma sintered ZrC–SiC and ZrC–SiC–CNT composites. *J Aus Ceram Soc* 2014, **50**: 76–82.